Freshwater Discharge, Sediment Transport, and Modeled Climate Impacts of the Final Drainage of Glacial Lake Agassiz

GARRY K. C. CLARKE

Department of Earth and Ocean Sciences, University of British Columbia, Vancouver, British Columbia, Canada

ANDREW B. G. BUSH

Department of Earth and Atmospheric Sciences, University of Alberta, Edmonton, Alberta, Canada

JOHN W. M. BUSH

Department of Mathematics, Massachusetts Institute of Technology, Cambridge, Massachusetts

ABSTRACT

A cold event at around 8200 calendar years BP and the release, at around that time, of a huge freshwater outburst from ice-dammed glacial Lake Agassiz have lent support to the idea that the flood triggered the cold event. Some suggest that the freshwater addition caused a weakening of the North Atlantic meridional overturning circulation (MOC) thereby reducing the ocean transport of heat to high northern latitudes. Although several modeling efforts lend strength to this claim, the paleoceanographic record is equivocal. The authors' aim is to use a coupled ocean–atmosphere model to examine the possibility that the two events are causally linked but that MOC reduction was not the main agent of change. It is found that the outburst flood and associated redirection of postflood meltwater drainage to the Labrador Sea, via Hudson Strait, can freshen the North Atlantic, leading to reduced salinity and sea surface temperature, and thus to increased sea ice production at high latitudes. The results point to the possibility that the preflood outflow to the St. Lawrence was extremely turbid and sufficiently dense to become hyperpycnal, whereas the postflood outflow through Hudson Strait had a lower load of suspended sediment and was buoyant.

1. Introduction

The early Holocene cooling event known as the "8.2 ka event" is the extreme event of the Holocene climate record in Greenland ice cores. In central Greenland, it was characterized by a ~3°C decrease in surface temperature and a modest reduction in snow accumulation rate (Thomas et al. 2007). Early contributions on the paleoenvironmental imprint of the 8.2 ka event tended to emphasize its hemispheric extent. This claim was bolstered by analyses of marine sediments in the tropical and North Atlantic (e.g., Hughen et al. 1996; Klitgaard-Kristensen et al. 1998), lake sediments in Europe and North America (e.g., von Grafenstein et al. 1998; Nesje and Dahl 2001; Spooner et al. 2002; Menounos et al.

2004; Veski et al. 2004), speleothems on the Arabian Peninsula (Fleitmann et al. 2003), and ice cores from tropical Africa (Thompson et al. 2002). Recent work has been less insistent about hemispheric extent, tending to emphasize the North Atlantic focus (e.g., Thomas et al. 2007) and spatial heterogeneity of the terrestrial signal (Seppä et al. 2007). For recent reviews see Alley and Ágústsdóttir (2005) and Rohling and Pälike (2005).

The cause of the 8.2 ka event remains controversial. A leading explanation is that the convective overturning of the North Atlantic Ocean was affected by the flux of freshwater to the Labrador Sea from the catastrophic drainage of an ice-dammed superlake that formed by the coalescence of glacial lakes Agassiz and Ojibway (e.g., Barber et al. 1999). Earlier abrupt climate change events seem to have been associated with ocean circulation changes in response to freshening of the North Atlantic, either by redirection of deglacial meltwater

Corresponding author address: Garry K. C. Clarke, Earth and Ocean Sciences, University of British Columbia, 6339 Stores Road, Vancouver, BC V6T 1Z4, Canada.
E-mail: clarke@eos.ubc.ca

(e.g., Clark et al. 2001; Teller and Leverington 2004; Tarasov and Peltier 2005) or by melting of icebergs episodically launched from the Laurentide Ice Sheet (LIS; e.g., Bond et al. 1992; Broecker 1994; Hemming 2004). Other workers view the flood as incidental to the cold event and propose that the cold event was caused by reduced solar insolation (van Geel et al. 2003) or stochastic variability of the climate system (Hall and Stouffer 2001; Goosse et al. 2002). Correct attribution of the cause of the cold event is absolutely crucial. If the cold event was caused by an ice age megaflood in the Northern Hemisphere, then the mechanism no longer poses a threat; if the cause is solar fluctuations or stochastic variability, then the possibility of a recurrence cannot be dismissed.

Estimates of the timing and duration of the 8.2 ka event present mixed messages. The best current estimate for the date of the Agassiz–Ojibway outburst is 8470 calendar (cal) years BP with 1-σ error range of 8160–8740 cal years BP (Barber et al. 1999), and the best current estimates of onset time and fine structure of the cold event come from Greenland ice core records. Based on analysis of ice cores from Greenland Ice Core Project (GRIP), Greenland Ice Sheet Project II (GISP2), North Greenland Ice Core Project (NGRIP), and Dye 3, Thomas et al. (2007) identify a 160-yr cold event that encloses a central event of 69-yr duration. The onset time for the 160-yr event is 8247 BP and is 8212 BP for the 69-yr event. The timing estimates for the flood and for the climate event have different reliability, the former being based on ^{14}C ages, to which a large reservoir correction has been applied, and the latter on direct counting of annual layers in ice cores. Evidence that there are two scales of variability associated with the 8.2 ka cooling has led some (e.g., Alley and Ágústsdóttir 2005; Rohling and Pälike 2005) to favor the idea that the centuries-long cooling cycle can be attributed to reduced solar activity and other influences, and only the decades-long central cold event might be attributed to the outburst flood. Obviously the issue of timing is critical because it is highly unlikely that any climate response to the flood was delayed by more than 5–10 yr.

The climate system switch that has received the greatest attention and for which there is the strongest evidence is that associated with changing the operation of the North Atlantic meridional overturning circulation (MOC). The engine for this circulation is sinking of dense (cold and saline) seawater at high northern latitudes and the brake, by this hypothesis, is the freshening of surface waters by various means, including atmospheric precipitation and melt from glaciers and icebergs. The Agassiz–Ojibway megaflood presents an exceptional opportunity for testing these ideas because

the volume of released freshwater and rate of delivery are well constrained. Several previous efforts to model the ocean response to the Lake Agassiz outburst can be faulted for either overestimating the volume of lake water released in the flood (e.g., Renssen et al. 2001, 2002, 2007; Wiersma and Renssen 2006) or for using a zonally averaged ocean model (Bauer et al. 2004), which necessarily avoids the question of how freshwater that is added at the ocean margins can migrate to the mid-Atlantic ocean. For these modeling studies the maximum MOC reduction ranges from around 40% to a near-complete shutdown. In terms of a proper representation of the freshwater forcing, the minimum forcing used by Wiersma et al. (2006) and that used by LeGrande et al. (2006) represent the best efforts thus far.

Recent paleochemical studies give evidence for cooling and freshening of the North Atlantic around the time of the flood (Ellison et al. 2006; Came et al. 2007), but paleochemical records of an associated MOC reduction have been lacking (Keigwin and Boyle 2000). Indicators such as δ^{13}C, δ^{14}C, Cd/Ca, and ^{231}Pa/^{230}Th in North Atlantic marine sediments record decreases in ocean ventilation and MOC strength coinciding with the Younger Dryas and earlier cold events (e.g., Boyle and Keigwin 1987; Lehman and Keigwin 1992; Hughen et al. 1998; McManus et al. 2004). Yet evidence for comparable decreases around 8.2 cal ka is less compelling. For example, Keigwin and Boyle (2000) concluded that "there are presently no paleochemical data that suggest the production of NADW was actually curtailed 8,200 years ago," and, more recently, Keigwin et al. (2005) stated "we find inconsistent evidence for a change at that time in deep ocean nutrient content." Using a sortable silt proxy for current strength at a site near the crest of the Gardar Drift, Bianchi and McCave (1999) found the flow at that site *increased* during the 8.2 ka event. Using the same proxy, more recent analyses of sediments deposited by Nordic seas overflows near the Gardar Drift (Ellison et al. 2006), the Eirik Drift (Kleiven et al. 2008), and the Reykjanes Ridge (Praetorius et al. 2008) indicate a "partial reduction in NADW overturning near the time of 8.2 ka, but not a 'shutdown'" (J. F. McManus 2008, personal communication).

The sparsity of evidence for a large reduction in poleward oceanic transport, in response to a seemingly ideal freshwater forcing, raises significant questions: 1) Was there no substantial change in ocean circulation, or was the change so short-lived that there is no clear record of the change? 2) If there was no substantial change in MOC, did the freshwater forcing induce a cold event by some other means? 3) Was the record of ocean changes masked, as has been suggested for the

North Atlantic $\delta^{18}O$ sedimentary record of the freshwater flood (LeGrande et al. 2006; C. Hillaire-Marcel et al. 2008)? 4) Was there simply a flood but no change in overturning and no other oceanic change sufficient to produce a cold event? The aim of our modeling study is to explore the possibility that there was no substantial reorganization of the ocean circulation in response to the freshwater outburst but there was nevertheless a climate response that resulted from other changes in the ocean and atmosphere.

2. Freshwater forcing

The megaflood from the Agassiz–Ojibway reservoir most likely began as a subglacial outburst, analogous to contemporary *jökulhaups* observed in Iceland (e.g., Björnsson 2003). Accepting this analog, the flood would have been produced by the rapid enlargement of a subglacial drainage conduit that diverted water flow from an eastward routing through the St. Lawrence basin to a northward one passing beneath the disintegrating Laurentide Ice Sheet and connecting to Hudson Strait (Fig. 1). The physical processes that govern such floods are reasonably well understood and can be represented in numerical models that simulate flood hydraulics (Clarke 2003), which can then be applied to predicting representative flood hydrographs for the Agassiz–Ojibway megaflood (Clarke et al. 2004). The detailed shape of the simulated flood hydrographs is somewhat dependent on the lake geometry at the time of the flood and on characteristics of the flood path that cuts across the Laurentide Ice Sheet. For forcing the ocean model the most important properties of the flood are the total released water volume and the flood duration, which Clarke et al. (2004) estimate as 151 000 km³ and 0.5 yr. We used their flood simulation results to guide the construction of a simple "canonical" hydrograph and rescale the amplitude and duration to yield the released water volume (Fig. 2c). For the canonical hydrograph $Q^*\{t^*\}$ the discharge volume is $V_{ref} = 54808$ km³. By introducing a scale factor $\alpha = \sqrt{V/V_{ref}}$, with $V = 151\,000$ km³, and applying this to rescale the canonical hydrograph we generate a flood hydrograph $Q(t) = \alpha Q^*(\alpha t^*)$ having the desired discharge volume.

The preflood discharge from the lake to the St. Lawrence drainage system can be inferred from tables in appendix A of Licciardi et al. (1999) (graphically summarized in Fig. 2 of Teller et al. 2002) and corresponds to roughly 0.1 Sv (1 Sv $\equiv 10^6$ m³ s⁻¹). This contribution adds to their 0.061-Sv estimated discharge from non-Agassiz sources to give a total preflood discharge through the St. Lawrence of 0.152 Sv. Before the
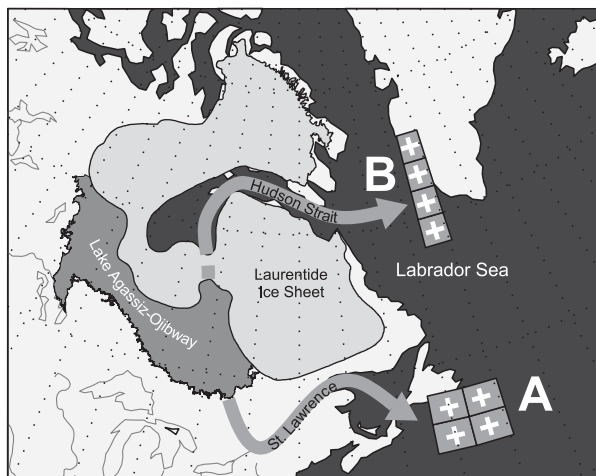

FIG. 1. Location of glacial Lake Agassiz and the Laurentide Ice Sheet at time of flood. The St. Lawrence River and Hudson Strait freshwater routings are indicated by arrows. Before the flood all water flowing into the lake is directed to the St. Lawrence drainage system. Following the flood all water flowing into the lake is routed through Hudson Strait. In the ocean model, which is coarsely resolved, these changes are effected by adding (+) freshwater at prescribed rates to the upper boundary of the indicated ocean model cells: the four A (+) cells near the tip of the St. Lawrence arrow (for the St. Lawrence outflow) and the four B (+) cells near the tip of the Hudson Strait arrow (for the Hudson Strait outflow).

flood onset, the estimated freshwater discharge through Hudson Strait was 0.055 Sv and after it was 0.171 Sv. A simple calculation indicates that this can be achieved by rerouting roughly 0.1 Sv from the St. Lawrence to Hudson Strait. Thus, in our study, the ocean forcing associated with the megaflood had two components: a long-lived northward rerouting of the base flow and a huge but short-lived flood pulse. More complicated forcing scenarios, involving resealing of the ice dam, partial refilling of the lake, and a second flood pulse, can be defended but will not be explored here.

Immediately before the flood onset, the outflow of water from Lake Agassiz was controlled by a bedrock spillway that fixed the lake level at around 230 m MSL (Clarke et al. 2004) and directed the overflow to the St. Lawrence River via the Kinojévis and Ottawa Rivers (Fig. 3), near the present border of Ontario and Quebec. This is the so-called Kinojévis stage of Lake Agassiz (Teller et al. 2002) and, judging from Fig. 2 of Leverington and Teller (2003), the lake was evolving extremely rapidly at this late moment in its history—the Kinojévis outlet was exploited for roughly 100 yr. Thus, unlike contemporary rivers, the Kinojévis outflow was traversing a landscape that had only recently been deglaciated and was geomorphically out of balance. In contrast, the
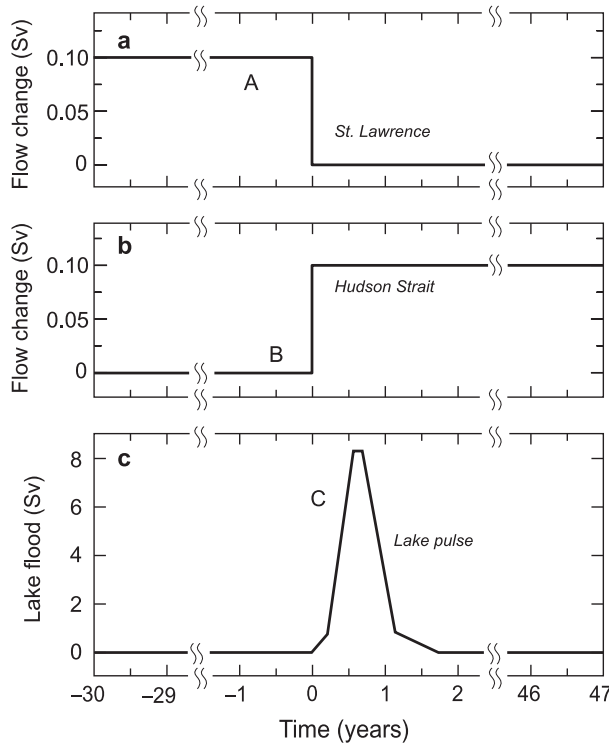
FIG. 2. Details of the freshwater forcing components. Time $t = 0$ yr is the time of the flood onset. (a) The change in base flow discharge through St. Lawrence River. (b) The change in base flow discharge through Hudson Strait. (c) The flood pulse from Lake Agassiz. The left ordinate applies to changes in the base flow.

postflood discharge that was diverted from the St. Lawrence system to Hudson Strait was flowing through the large settling pond of Hudson Bay and, en route, could deposit much of its sediment load. In a subsequent section we quantify the argument that discharge from Lake Agassiz to the St. Lawrence system, via the Kinojévis routing, was likely to be highly turbid whereas the same discharge routed toward Hudson Strait was not.

The separate components of the freshwater forcings summarized in Fig. 2 are the base flow to the Gulf of St. Lawrence (A in Fig. 2a), the base flow to Hudson Strait (B in Fig. 2b), and the flood pulse from Lake Agassiz (C in Fig. 2c). The forcing A + B + C represents the combined effects of rerouting and the release of stored water in the lake. The B + C forcing (no preflood flow to the Gulf of St. Lawrence) is appropriate to the case where the discharge to the St. Lawrence is highly turbid and possibly hyperpycnal, an idea that is explored in the next section. The A + B + C and B + C forcings can be viewed as end members of a continuum of possible models $\varepsilon A + B + C$ where $0 \leq \varepsilon \leq 1$ and ε decreases with increasing suspended sediment load.

3. Effect of suspended sediment

In this section we consider the possibility that, around the time of the flood, the sediment load in the St. Lawrence discharge was extremely high and that the freshwater delivered to the Gulf of St. Lawrence was so dense that it could not form a low-salinity upper-ocean layer. In contrast, the freshwater outflow through Hudson Strait, after and possibly during the flood phase, had a much lower sediment load and could remain at the top of the water column. Marine sediment core MD99–2221, retrieved from the St. Lawrence estuary (Fig. 3), confirms that the sedimentation rate at the time immediately preceding the 8.2 cal ka event (i.e., before $\sim$7700 ^{14}C yr BP) was extremely high (St-Onge et al. 2003), as it would be if the discharge carried a high sediment load.

a. Hydraulic modeling

The possibility that the turbidity of freshwater flowing to the ocean might determine whether the water can act as an agent of climate variability is a complication that has only recently received scientific attention (Tarasov and Peltier 2005; Aharon 2006; Roche et al. 2007). Here we demonstrate how paleohydraulic and paleotopographic information can be incorporated in runoff models that can then be used to assess the suspended sediment load. In terms of Cartesian map coordinates, the water flow path can be written $[x(s), y(s), z(s)]$ where s is an along-path distance coordinate. In this system the cross-sectional area of the water conduit is $S(s, t)$, the channel floor elevation is $Z_B(s)$, the maximum water depth is $H(s, t)$, the cross-sectionally averaged water velocity is $v(s, t)$, and t is time. The equations governing the flow are

$$\frac{\partial S}{\partial t} = -\frac{\partial}{\partial s}(vS) + \sum_{k=1}^{N} Q_k \delta(s - s_k), \qquad (1)$$

$$\frac{\partial v}{\partial t} = -\frac{\partial}{\partial s}\left[\frac{1}{2}v^2 + g(H + Z_B)\right] - \frac{\tau_0 P}{\rho_w S}, \qquad (2)$$

where (1) is the water continuity equation and (2) the momentum equation. In Eq. (1), the summation term accounts for tributary inflows of magnitude Q_k (m^3 s^{-1}) at discrete points s_k along the channel; $\delta(s - s_k)$ represents a Dirac delta function. In Eq. (2), $g = 9.80$ m s^{-2} is the gravity acceleration, $\tau_0(s, t)$ is the shear stress acting at the channel walls, $P(s, t)$ is the wetted perimeter of the channel, and $\rho_w = 1000$ kg m^{-3} is the density of freshwater. The wall stress is related to the flow velocity by the expression $\tau_0 = \frac{1}{8}f_R \rho_w v^2$, where f_R is a dimensionless roughness parameter; f_R is related to the Manning roughness parameter n by $f_R = 8gn^2/R_H^{1/3}$,
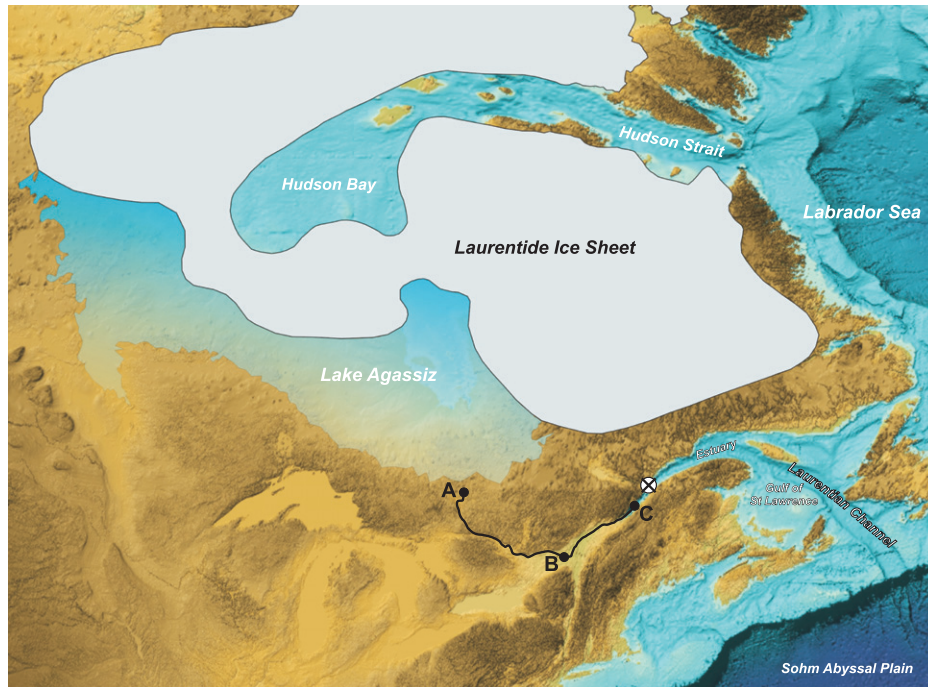
FIG. 3. Topographic setting of Lake Agassiz and its preflood drainage pathway. The solid black line ABC indicates the 845-km-long drainage pathway from the lake to the St. Lawrence estuary. Segment AB of the curve indicates the route along the Kinojévis and Ottawa Rivers; segment BC follows the present-day routing of the St. Lawrence River. Point B (220 km downstream from point A) is located at the confluence of the flows from Lake Agassiz and from non-Agassiz sources. The site of the MD99–2221 marine sediment core is marked (white circle with ×).

where $R_H = S/P$ is the hydraulic radius of the channel. The discharge is simply $Q = vS$ and, at steady state, is constant at Q_0 along the entire length of the channel if inflow from tributary channels is negligible. To characterize the hydraulic roughness of the channel, we take $n = 0.03$ m$^{-1/3}$ s, a representative value for rivers. For the upstream ($s = 0$) boundary conditions we take $S(0, t) = S_0$ and $v(0, t) = Q_0/S_0$, where Q_0 is the paleohydraulic discharge along the channel (e.g., 0.1 Sv) and S_0 is chosen to make $v(0, t)$ small (e.g., 1 mm s^{-1}). The channel evolution equations are integrated using the numerical method of lines (Schiesser 1991) and MATLAB solver ode15s until a steady state is attained. Following this modeling approach, we can compare the paleohydraulic conditions along the Kinojévis–St. Lawrence and Hudson Bay–Hudson Strait drainage routings.

The results of the Kinojévis–St. Lawrence discharge simulations are summarized in Fig. 4. To simplify the plot we introduce a dimensionless distance variable $s^* = s/L$, where L is the total pathlength. Rather than adopt the simplified discharge forcings (Fig. 2) that will be used in the ocean modeling, we apply the exact values proposed in appendix A of Licciardi et al. (1999). The confluence of the upper St. Lawrence drainage with the Kinojévis drainage is accounted for by taking $Q_0 = 0.0915$ Sv (representing the preflood outflow from Lake Agassiz) and $Q_1 = 0.0609$ Sv with $s_1 = 220$ km to account for the inflow of water from the upper St. Lawrence catchment. The total preflood discharge to the St. Lawrence estuary is thus $Q_0 + Q_1 = 0.1524$ Sv; during and after the flood it drops to 0.0609 Sv.

The total pathlength for the flow from Lake Agassiz to the St. Lawrence estuary is 845 km, and the elevation drop was around 230 m at the time of the flood but is ~275m in Fig. 4a because we use modern topography for this computation. (Uncertainties in paleotopography and early Holocene sea level would introduce minor changes in the discharge simulations that would not affect the principal conclusions of this study.) For the upper reaches of the flow ($0.1 < s^* < 0.35$) the path is steep (Fig. 4a) and the channel area is small (Fig. 4b). The resulting water velocity (Fig. 4c) is very fast for a river, as high as 5–6 m s^{-1}, and the associated shear stress on the channel walls (Fig. 4d) reaches 1.1 kPa. The flow Reynolds number (Fig. 4e), which indicates the degree of shear turbulence, ranges from 10×10^6 to 150×10^6, and the calculated water transit time (Fig. 4f) from Lake Agassiz to the St. Lawrence estuary is roughly 13 days.
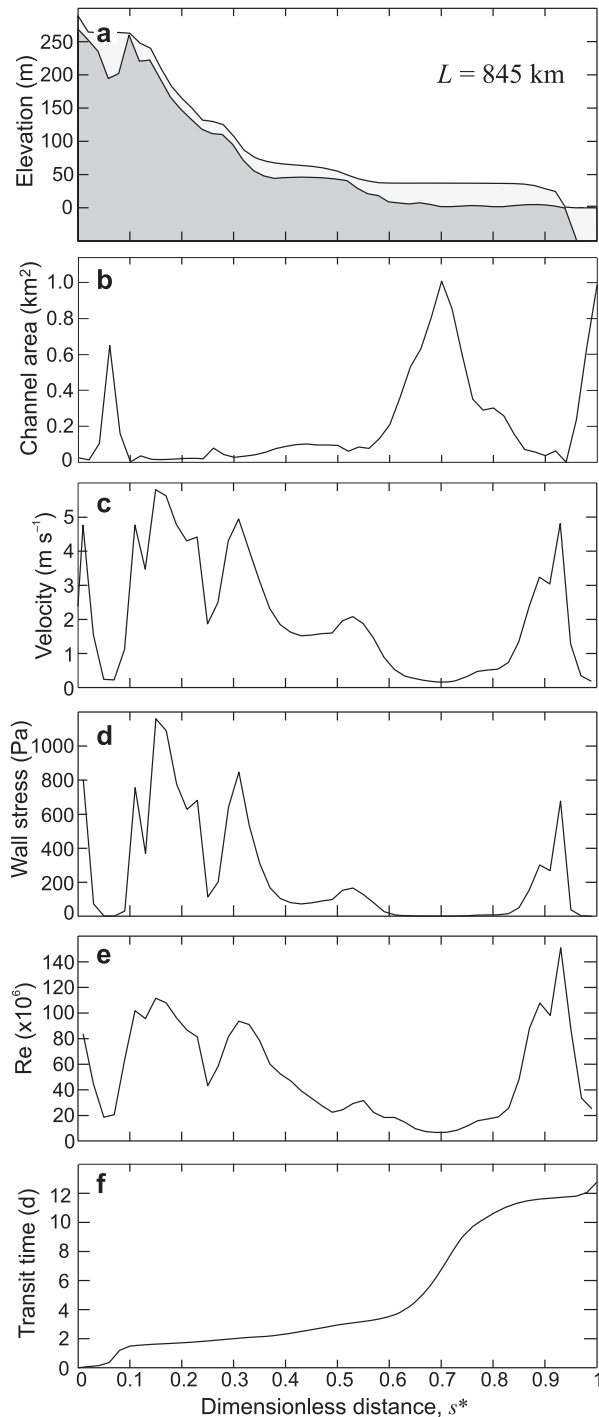
FIG. 4. River simulation results for Kinojévis–St. Lawrence rout-ing with $Q = 0.1542$ Sv flowing into the St. Lawrence estuary. The overflow from Lake Agassiz is taken as $Q_0 = 0.0915$ Sv to which is added, at a downstream distance $s_1 = 220$ km, a contribution $Q_1 = 0.0609$ Sv from the upper St. Lawrence River. The dimen-sionless distance is $s^* = s/L$ where s is the distance in km and $L = 845$ km is the river length. (a) River profile (m MSL), (b) channel cross-sectional area (km²), (c) water velocity (m s⁻¹), (d) wall stress (Pa), (e) Reynolds number, and (f) transit time from lake (days).

Sediment availability for the Kinojévis routing is presumed to be very high because the Kinojévis spillway was short lived, and water following this routing was traversing a landscape that had only recently been de-glaciated and was not near geomorphic equilibrium with respect to surface water flow. According to the ice margin reconstructions of Dyke et al. (2003), the upper 75% of the AB (Fig. 3) segment of the Kinojévis–Ottawa–St. Lawrence rivers pathway was ice covered at 13.45 ka BP, 50% at 12.7 ka BP, and around 0% at 10.75 ka BP and thereafter. The drainage reconstruction of Teller and Leverington (2004, their Table 1) indicates that Lake Agassiz overflow routings that followed the Ottawa River valley (among these the Kinojévis rout-ing) into the St. Lawrence River were active continu-ously from 8.67 to 8.45 ka BP. Prior to 8.67 ka BP a different drainage pathway was exploited for overflow from Lake Agassiz precursors.

Applying a similar analysis to the Hudson Strait routing (and simplifying this system by viewing it as a river channel that starts at the entrance to Hudson Strait and terminates where it debouches into the Labrador Sea), we obtain the results presented in Fig. 5. (The shape of the graphs, though not the scaling, is identical or virtually identical for both the flood and postflood simulations. For efficiency of exposition, the right or-dinates apply to the flood case and the left ordinates to the postflood case.) Viewed as a river channel, Hudson Strait has negligible surface slope and a very large cross-sectional area (Figs. 5a,b). As a result, the flow velocity and wall stress (Figs. 5c,d) are much lower than for the Kinojévis–St. Lawrence channel: less than 0.9 m s⁻¹ and 10 Pa during the flood and less than 30 mm s⁻¹ and 11 mPa following it. Owing to the large length scale, the flow for both situations is highly turbulent, with Reyn-olds numbers ranging from 50×10^6 to 350×10^6 during the flood and 1×10^6 to 12×10^6 after it. The calculated transit time through Hudson Strait varies from 60 days during the flood to 2000 days following it.

b. Sediment entrainment and deposition

The hydraulic simulations summarized above can be used to assess the conditions for sediment entrainment and deposition that prevailed before, during, and after the Lake Agassiz outburst flood. Consider the forces acting on a spherical sediment grain of diameter D_p at rest on the channel floor. The particle is acted upon by a gravitational force $F_g = \frac{\pi}{6}(\rho_s - \rho_w)gD_p^3$ and a dy-namic pressure force F_d, which at low values of the particle Reynolds number $Re_p = \rho_w v D_p/\mu$ is given by $F_d = 3\pi\rho_w D_p/\mu$ and at high values by $F_d = \frac{1}{8}C_D\rho_w v^2 D_p^2$, where ρ_s is the grain density and C_D is a form drag co-efficient for the particle. For simplicity, we take $F_d > F_g$

TABLE 1. Summary of discharge scenarios.

Label	Description
A	Preflood outflow (1 Sv) following St. Lawrence routing (-30 to 0 yr)
B	Postflood outflow (Sv) following Hudson Strait routing (0 to 47 yr)
C	Lake pulse of 151 000 km^3 (0 to 1.66 yr)
B + C	Lake pulse plus postflood outflow through Hudson Strait (0 to 47 yr)
A + B + C	Preflood outflow following St. Lawrence followed by lake pulse and postflood outflow through Hudson Strait (-30 to 17 yr)

as the condition for particle entrainment, which leads to the result that

$$D_p^+ = \begin{cases} \left[\dfrac{18\mu v}{(\rho_s - \rho_w)g} \right]^{\frac{1}{2}} & \text{low } \mathrm{Re}_p \\[2ex] \dfrac{3C_D \rho_w v^2}{4(\rho_s - \rho_w)g} & \text{high } \mathrm{Re}_p \end{cases} \qquad (3)$$

is the largest particle size that can be entrained when the flow rate is v. For subsequent calculations we shall assume $\rho_s = 2700$ kg m^{-3} and $C_D = 0.5$. The threshold between low and high Re_p end members lies at $\mathrm{Re}_p \approx 1$.

Next we turn to the problem of particle settling in a turbulent flow. Martin and Nokes (1988) examined the effect of turbulence on sedimentation and arrived at the remarkably simple result that the sediment residence time in the water column depends on the particle settling speed, and on whether or not the outflow is turbulent. If it is turbulent, the particle concentration decreases exponentially with an e-folding time of H/v_s, where H is the depth and v_s the settling speed (which will take one of two forms according to whether the particle settles at low or high Reynolds number). This e-folding time may now be considered as the residence time in the water column. If, conversely, the outflow is laminar, then the particles will simply settle out linearly with time at a speed v_s, so the characteristic settling time is H/v_s. We have reworked this result, for the case of turbulent flow, so that it can be applied to flow through a channel with variable discharge $Q(s)$, cross-sectional area $S(s)$, and depth $H(s)$, and obtain

$$\frac{dc_p^*}{ds} = -\frac{D_p^2(\rho_s - \rho_w)g}{18\mu} \frac{S c_p^*}{QH}, \qquad (4)$$

where $c_p^* = c_p(s)/c_p(0)$ is the sediment concentration for particles of size D_p, relative to the concentration at $s = 0$, and $\mu = 1.787 \times 10^{-3}$ Pa s. An assumption of the Martin and Nokes theory is that the particle settling rate is slow relative to the speed of the turbulent flow. Thus large fast-settling particles will settle out faster than predicted by Eq. (4) and the expression sets an upper bound on suspended sediment concentrations if along-flow entrainment is neglected.

c. Conditions along the Kinojévis–St. Lawrence routing

Our purpose is to assess the possibility that the water following the Kinojévis–St. Lawrence routing was so sediment-laden that it was hyperpycnal relative to ocean water. Were this the case, the discharge component A would not contribute to the freshening of the ocean surface and this would provide a justification for favoring the B + C forcing over the A + B + C forcing. Figure 6a uses Eq. (3) to summarize the entrainment conditions along the Kinojévis–St. Lawrence routing. The largest particle size that can be entrained by the flow varies with distance along the channel from a maximum of $D^+ \approx 1$ m near the lake to a minimum of 1mm at $s^* = 0.65$. The implication is that all sediment smaller than gravel size can be entrained by the flow. Figure 6b uses Eq. (4) as a basis for assessing the conditions for particle sedimentation in the absence of particle entrainment. Most clay-size particles that entered the flow near $s^* = 0$ would remain in suspension, whereas most sand-size particles would settle out upstream from $s^* = 0.1$. Clearly, the actual situation is dominated by the entrainment process and, though sand-size particles cannot remain long in suspension, they will be vigorously reentrained by the flow, and, consequently, the water delivered to the St. Lawrence estuary (Fig. 3) would contain gravel-size particles ($D_p > 2$ mm) as well as sediment of smaller grain size.

Based on the above reasoning, the likelihood that the flow to the St. Lawrence estuary was densely laden with suspended sediment, during the interval that the Kinojévis spillway was exploited, seems high. The strict condition for hyperpycnal flow is that $\rho > \rho_{sw}$ where ρ is the density of sediment-laden water and ρ_{sw} that of seawater. A representative density for seawater is $\rho_{sw} = 1035$ kg m^{-3} and this corresponds to a $\sim$35 kg m^{-3} sediment load—high but not impossibly high for glacial meltwater. Based on laboratory experiments, Parsons et al. (2001) argue that the $\rho > \rho_{sw}$ condition can be far too stringent and that "hyperpycnal plumes can be formed with sediment concentrations as low as 1 kg m^{-3} under realistic ocean conditions." Although the result seems surprising, the settling process involves the development
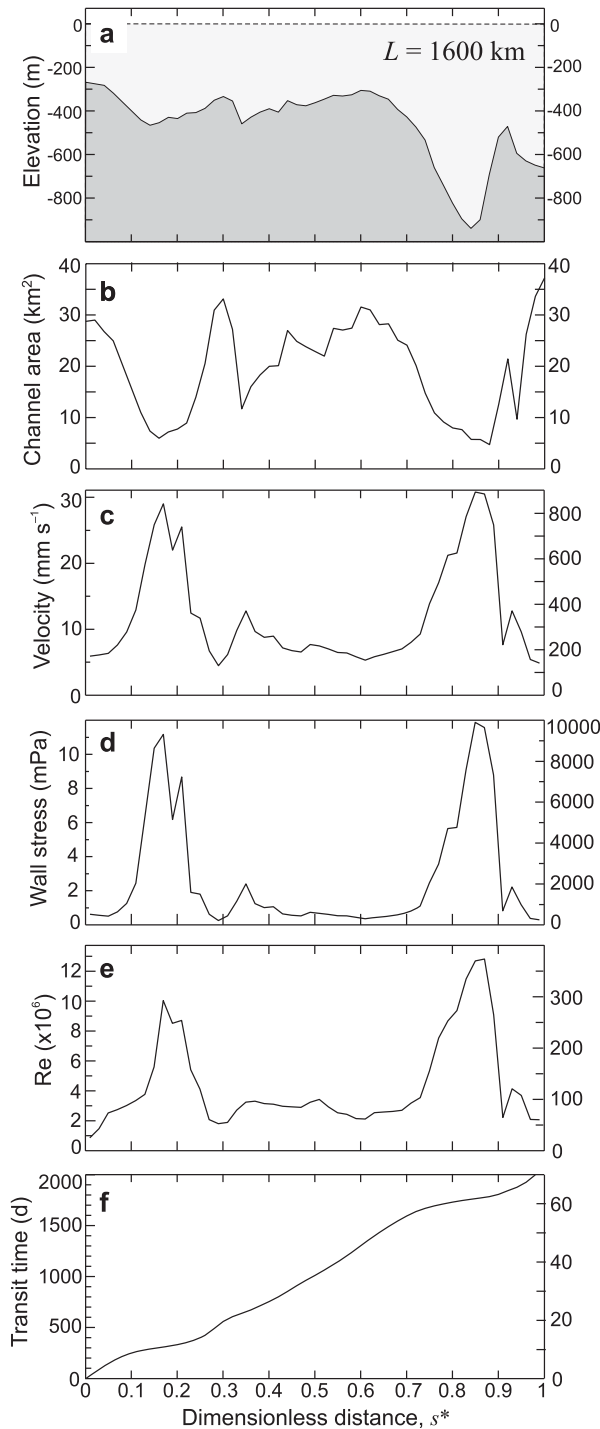
FIG. 5. Simulated outflow through Hudson Strait during (right ordinate) and following (left ordinate) the outburst flood. The assumed flood discharge is $Q = 5$ Sv and the assumed postflood discharge is $Q = 0.1718$ Sv. The dimensionless distance is $s^* = s/L$, where s is the distance in km and $L = 1600$ km is the length of the channel through Hudson Strait. (a) Channel profile (m MSL), (b) channel cross-sectional area (km^2), (c) water velocity (mm s^{-1}), (d) wall stress (mPa), (e) Reynolds number, and (f) transit time from lake (days).
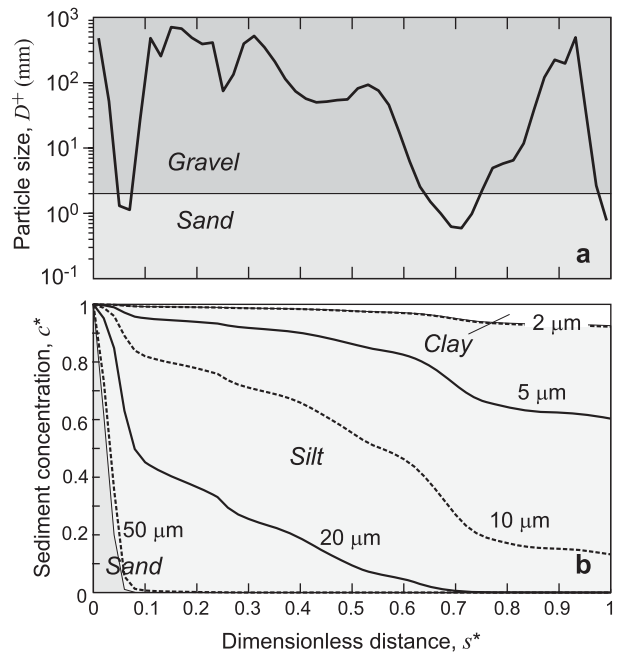

FIG. 6. Sedimentation conditions for the Kinojévis routing. Results are for the Kinojévis plus inflow from upper St. Lawrence tributary. The overflow from Lake Agassiz accounts for 0.0915 Sv and discharge from the tributary channel is 0.0609 Sv applied at $s = 220$ km. The horizontal axis is dimensionless distance $s^* = s/L$ where s is the distance in km and $L = 845$ km is the total channel length. (a) Conditions for particle entrainment. The diameter D^+ of the largest spherical particle that can be entrained at a given downstream distance in the channel. (b) Conditions for particle settling.

of convective instability at the base of the overlying layer of fresh, turbid water. The significance of this process is that it counteracts the tendency for sediment to separate from the freshwater in which it is suspended and drives both freshwater and sediment down the water column. Depending on the sediment load, there is a spectrum of possibilities between the fully hyperpycnal and fully hypopycnal end members and, under certain circumstances, hyper- and hypopycnal plumes can coexist.

d. Sediment deposition in Hudson Bay

Although the postflood baseline discharge through Hudson Strait is comparable to the preflood baseline discharge to the St. Lawrence estuary, suspended sediment load for the two systems could differ significantly. A very rough estimate of the turnover time of Lake Agassiz water in Hudson Bay is $t_{res} = V_{res}/Q_{in}$. Taking $V_{res} = 86\,000$ km^3 (roughly the present volume of Hudson Bay, excluding Hudson Strait and Foxe Channel) and $Q_{in} = 5$ Sv (the flood discharge from Lake Agassiz) one gets $t_{res} = 200$ days. Following the flood, with $Q = 0.1718$ Sv

the estimated turnover time is 5800 days. Although these are long times, the settling time for fine particles is also long. Figure 7 (solid curve) shows the Stokes' law settling time $t_p = 18d\mu/gD_p^2(\rho_s - \rho_w)$ for a particle of diameter D_p and a settling distance of $d = 100$ m, roughly the mean water depth in Hudson Bay. Also indicated on the diagram are the residence times that correspond to the flood and postflood discharges through Hudson Bay. For a flood discharge of $Q = 5$ Sv, silt-size and larger particles will have sufficient time to settle out before they reach the entry to the Hudson Strait channel; for a postflood discharge of $Q = 0.1718$ Sv large clay-size particles have sufficient time to settle out.

e. Conditions in Hudson Strait

Relative to Hudson Bay, Hudson Strait represents a flow constriction and site where entrainment of bottom sediment could be significant. Figure 8a shows the modeled entrainment conditions in Hudson Strait during (dashed line) and following (solid line) the flood. During the flood it is possible to entrain coarse sand and gravel-sized particles in Hudson Strait; following the flood these large particle sizes cannot be mobilized but there is sufficient flow to entrain fine sand and smaller particles. The fate of this sediment depends on the sedimentation conditions along the channel (Figs. 8b,c). During the flood (Fig. 8b), sand-size particles entering Hudson Strait would settle out over a fairly short distance ($s^* \approx 0.1$) but fine silt and clay-size particles would remain in suspension. Following the flood (Fig. 8c), medium- and coarse-grained silt can settle out. The combined effects of the particle entrainment and settling conditions in Hudson Strait suggest that, during the flood, sand-size and smaller particles can be delivered to the Labrador Sea; following the flood, only clay and fine-grained silts are transported through Hudson Strait to the Labrador Sea.

From this assessment, we conclude that it is possible that Hudson Strait outflow carried a high sediment load during the flood but was unlikely to do so following it. This conclusion is consistent with observations of flood-contemporaneous features in marine sediment cores. In northern Hudson Bay and western Hudson Strait, St-Onge and Lajeunesse (2007) report a sequence of hyperpycnites within the reddish layer (Kerwin 1996) that is characteristic of deposits from Lake Agassiz outburst(s). In the Labrador Sea, Hillaire-Marcel et al. (2007) find a twin layer of carbonate rich turbidites that they attribute to the flood.

f. Caveats

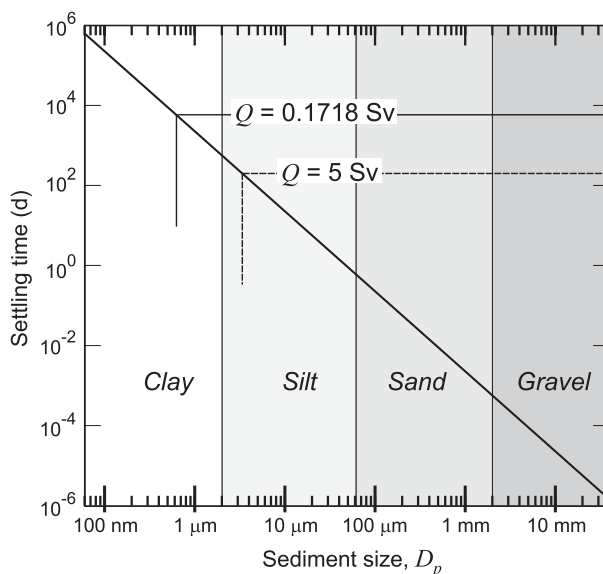Note that the above discussion of entrainment and settling is based on back-of-the-envelope calculations:

FIG. 7. Settling of suspended sediment in Hudson Bay. The thick solid line indicates the calculated settling times over a range of sediment diameters and an assumed settling distance of 100 m. The estimated water estimated residence time in Hudson Bay is 200 days for a flood discharge of 5 Sv through Hudson Bay and 5800 days for a postflood discharge of 0.1718 Sv.

more sophisticated models of particle resuspension and settling in riverine outflows are the subject of ongoing research. Our examination of the conditions for sediment entrainment implicitly assumes that an unlimited supply of sediment is available. This would not be the case if the landscape was already denuded of sediment or if the only available sediment was too coarse to be entrained by the flow. Treating Hudson Bay as a settling pond and Hudson Strait as a river represents a massive simplification. The modern ocean circulation through Hudson Bay is known to be complex and strongly influenced by tidal and Coriolis forces (Saucier et al. 2004; Straneo and Saucier 2008). Likewise, the assumption that the water mass is well mixed over the channel cross-section is unrealistic for the kind of stratified flow that is likely to develop during freshwater floods through the Hudson Bay–Hudson Strait system.

4. Modeled climate response

To calculate the ocean and atmosphere responses to the various freshwater forcing scenarios, we employ a fully coupled general circulation model of the atmosphere and ocean developed at the Geophysical Fluid Dynamics Laboratory (GFDL) in Princeton, New Jersey. The atmosphere model is spectral with rhomboidal (r30) truncation and 14 vertical levels using a terrain-following sigma coordinate system (Gordon and Stern
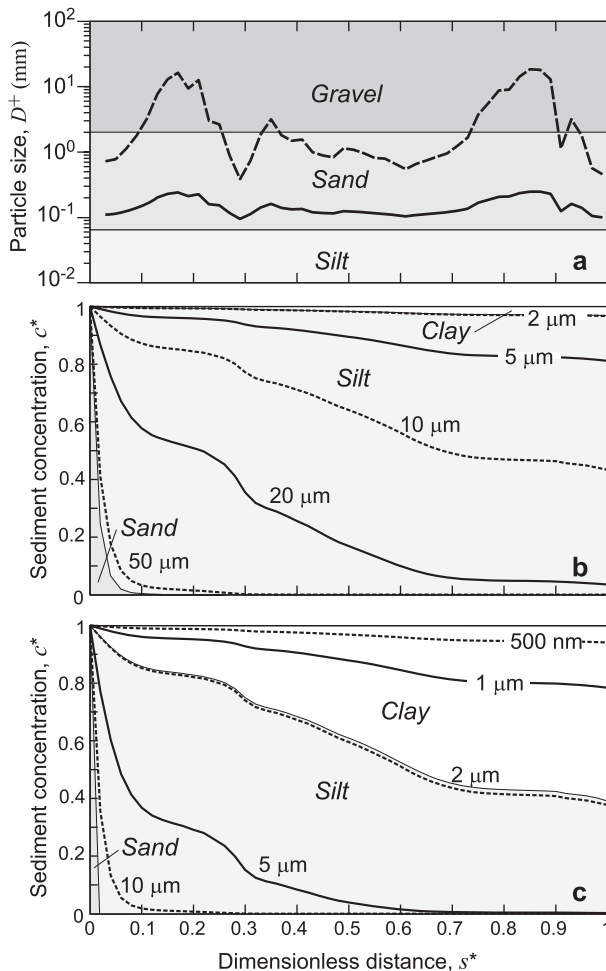
FIG. 8. Sedimentation conditions for the Hudson Strait channel. For the flood the total discharge through Hudson Strait is taken as 5 Sv. Following the flood the postflood discharge through Hudson Strait is taken as 0.1718 Sv. The horizontal axis is dimensionless distance $s^* = s/L$ where s is the distance in km and $L = 1600$ km is the total channel length. (a) Conditions for particle entrainment during the flood (dashed line) and immediately following it (solid line). The diameter D^+ of the largest spherical particle that can be entrained at a given downstream distance in the channel. (b) Conditions for particle settling during the flood. (c) Conditions for particle settling immediately following the flood.

1982). It has a full hydrologic cycle, predicted clouds (Wetherald and Manabe 1988), and seasonal radiation. Topography in the model is consistent with the spectral resolution and is spectrally smoothed to reduce Gibbs oscillations associated with the finite truncation numbers (e.g., Navarra et al. 1994). The ocean model is the Princeton Modular Ocean Model (MOM 2; Pacanowski 1995) and has a resolution of 3.75° in longitude, 2.0° in latitude, 15 unevenly spaced vertical levels, and a rigid lid. The physical configuration (in terms of grids and resolution) is identical to the GFDL_R30 model ana-

lyzed in Stouffer et al. (2006). However, the diffusive mixing scheme (Stouffer et al. 2006, their Table 1) is replaced by the Pacanowski and Philander (1981) dynamic vertical mixing scheme, which is based on the local Richardson number (and not diffusion), together with convective adjustment for gravitational instability. The thermodynamic sea ice module is based on Fanning and Weaver (1996). For the control run, orbital parameters are set to those for 8200 cal years BP (Berger and Loutre 1991), and atmospheric CO_2 is fixed at 260 ppmv (Indermühle et al. 1999). We use Levitus (1982) for the salinity of both modern and 8200 cal years BP control runs, neglecting the ~0.15-psu difference that would be associated with ~15 m lower sea level of the early Holocene (Peltier 1998, Fig. 37). Except for remnants of the LIS, modern topography and land surface albedo are assumed, together with modern sea level and riverine freshwater fluxes. The paleotopography for the LIS is found by linear interpolation between the 1000-yr intervals of ICE4G (Peltier 1994) and over these regions the surface albedo is fixed at 0.6, though this can increase if there is fresh snow cover. Freshwater additions associated with the Lake Agassiz flood and the rerouting of glacial meltwater (Fig. 1) are assumed to have no salinity (0 psu) and a temperature identical to that of the ocean grid cell to which the water is added. Salinity is monitored at every time step to detect negative values and set these to zero.

Simulations were run on a Silicon Graphics, Inc. (SGI), Origin 2400 (6 processors) and the run time is about 1 yr day^{-1}; that is, the three simulations presented here each take nearly 50 days to execute.

In some ocean modeling studies, diapycnal diffusivities are set artificially high in order to obtain a desired value for the meridional overturning circulation. Such high values are not justified from observations (e.g., Ledwell et al. 1998; Egbert and Ray 2000) and they tend to erode the tropical thermocline sufficiently that important global phenomena such as ENSO are poorly reproduced (e.g., Meehl et al. 2001; Bush 2007). The vertical mixing scheme used here dramatically improves the model's ability to simulate ENSO, both in terms of frequency and magnitude (Bush 2007); additionally, an internal wave mixing scheme has also been incorporated to account for deep ocean mixing (e.g., Jayne and St. Laurent 2001; Simmons et al. 2004).

To introduce the effect of elevated freshwater discharge through the St. Lawrence River system, prior to the lake outburst at $t = 0$, the control was run from $t = -50$ yr to $t = -30$ yr, at which time a discharge of 0.1 Sv was added to the control value. At $t = 0$ the flood is released to Hudson Bay and, simultaneously, the freshwater inputs to the ocean cells indicated in Fig. 1

are adjusted to account for a 0.1-Sv reduction of the St. Lawrence discharge (if the A component of freshwater forcing is included) and a 0.1-Sv increase in the freshwater discharge through Hudson Strait (if the B component of freshwater forcing is included). We find that the modeled mid-Atlantic response to sustained 0.1-Sv forcings is essentially insensitive to whether the water addition occurs at the four A(+) cells or the four B(+) cells in Fig. 1.

These simulations are analogous to those performed for the Coupled Model Intercomparison Project (CMIP; Stouffer et al. 2006) but here, based on geologic evidence, the freshwater addition is geographically targeted. As discussed in Stouffer et al. (2006), the location of deep convection can vary from model to model, although our results indicate that the advection of the surface fresh layer takes it over all sites of contemporary North Atlantic convection. Having an active atmospheric component in the model is likely to be critical to generating a realistic climate response, given the atmosphere's dominant role in meridional heat transport (e.g., Trenberth and Caron 2001; Seager and Battisti 2007; Seager et al. 2002). Differences between our modeled sensitivity to freshwater additions and those found in the CMIP intercomparison are likely to be associated with the actively coupled atmosphere (not a feature of all the intermediate complexity models) and our preference for the Pacanowski and Philander (1981) dynamic mixing scheme.

a. Temporal perspective

Figure 9 shows spatially averaged time series of the change in monthly mean surface air temperature at selected sites in the Northern Hemisphere. Spatial averaging is performed over areal patches (see caption for details) for the A + B + C, B + C, and C forcings. The smoothed time series for central Greenland (Fig. 9a) shows a 5°C drop in mean annual temperature in response to forcings C and B + C with the main difference being that the recovery from C proceeds rapidly at $t \approx 7.5$ yr, whereas there is no recovery from B + C in 47 postflood years. For the western British Isles (Fig. 9b), the drop in mean annual temperature is around 3°C for the C and B + C forcings and the recovery from C starts around 6 yr after the flood onset. As for Greenland, there is no recovery from the B + C forcing after 47 yr.

When the system is preconditioned for 30 yr by St. Lawrence outflow (A + B + C in Fig. 9), the switch to a cold state begins around $t = -25$ yr and the system is completely entrenched in a cold state by the time the flood occurs at $t = 0$. The flood and rerouting events have virtually no additional impact because sea ice and cold temperatures have already spread across the North At-
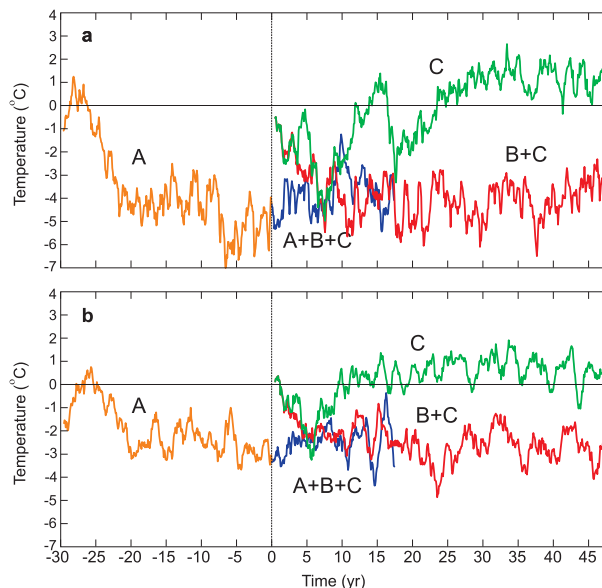

FIG. 9. Time series of modeled monthly averaged surface temperature change for three experiments. Forcing A (orange curves; from $t = -30$ yr to $t = 0$) is the response to 30 yr of preconditioning by 0.1 Sv of St. Lawrence outflow; forcing C (green curves; 47 yr duration) are for the outburst flood only; forcing B + C (red curves; 47 yr duration) for the flood followed by 0.1 Sv of outflow through Hudson Strait; forcing A + B + C (blue curves; 17 yr duration) is for 30 yr of preconditioning ($-30 \leq t \leq 0$) by 0.1 Sv of St. Lawrence outflow, a flood at $t = 0$, followed by 0.1 Sv of outflow through Hudson Strait. (a) Greenland change (averaged 70°–80°N, 60°–50°W). (b) British Isles change (averaged 50°–58°N, 10°W–0°).

lantic by the time of the flood onset. Once the cold switch has been thrown the system responds weakly to additional freshwater forcing. It was this result that prompted our interest in the turbidity of the St. Lawrence flow and the suitability of the B + C forcing.

b. Spatial perspective

The results of the coupled model study for the B + C forcing are summarized in Figs. 10–13. Figure 10 shows the modeled changes in sea surface temperature (SST), sea surface salinity (SSS), surface air temperature (SAT), sea ice thickness, precipitation, and snowfall. These maps represent time-averages rather than snapshots and are obtained by averaging over postflood years 10–47 with the aim of suppressing the transient response to the lake pulse and isolating the sustained, though fluctuating, response to the postflood outflow through Hudson Strait. Regions of greatest ocean cooling (around 4°–6°C in Fig. 10a) are located in the Greenland Sea, the Norwegian Sea, and the Barents Sea. Increased SST is predicted for the northeast coast of the United States and in the Arctic Ocean north of Siberia. The map
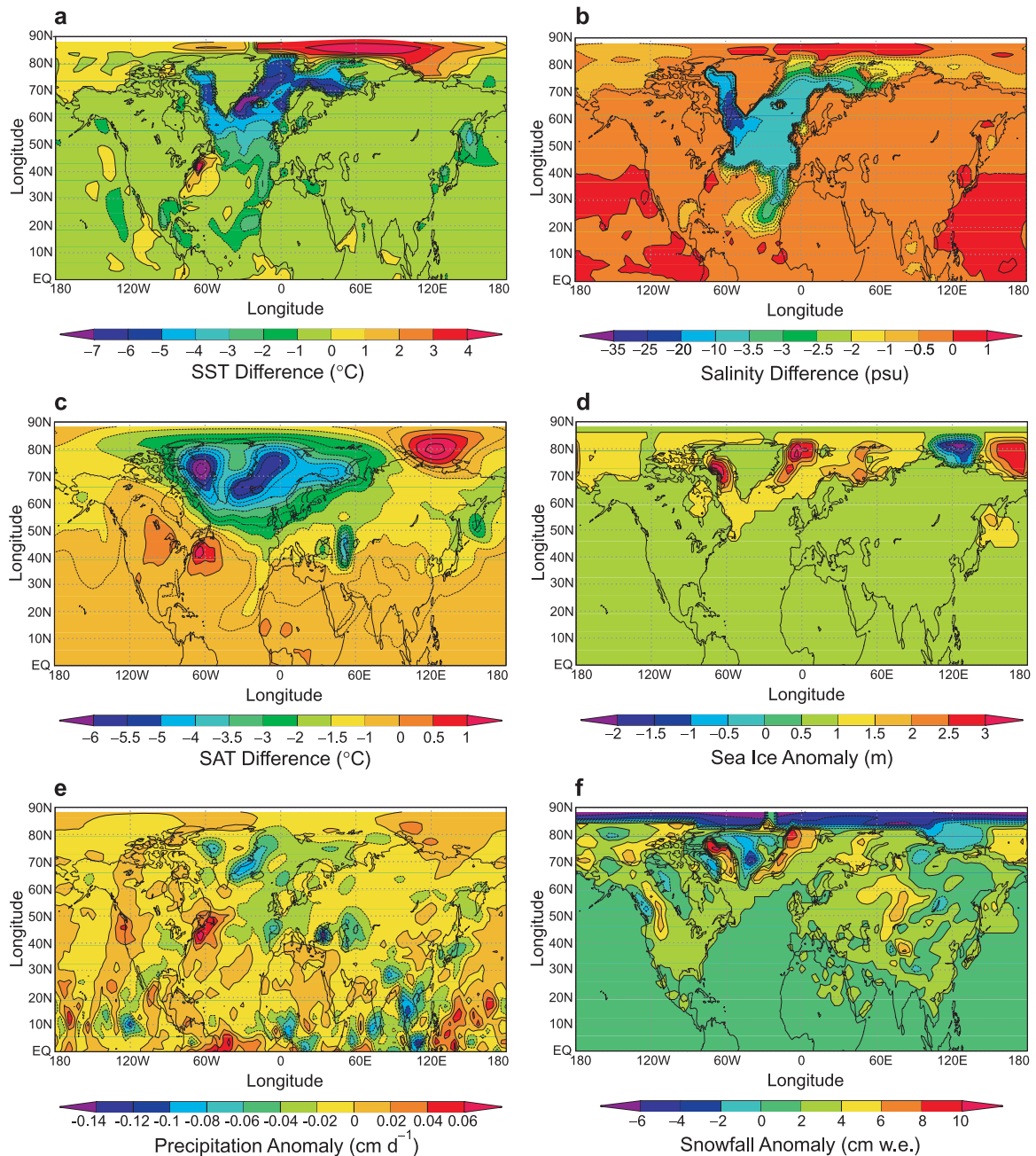
FIG. 10. Response of coupled atmosphere–ocean model to freshwater forcing B + C. Results are averaged over postflood years 10–47. (a) Change in sea surface temperature (°C). (b) Change in surface salinity of ocean (psu). (c) Change in surface air temperature (°C). (d) Change in sea ice thickness (m). (e) Change in precipitation (cm day^{-1}). (f) Change in snowfall (centimeters water equivalent).

of sea surface salinity differences (Fig. 10b) shows that the entire North Atlantic Ocean north of 45°N is conspicuously freshened by the Agassiz flood, and there is a surprising southward extension of freshwater along the west coast of Portugal, Spain, and Morocco carried by the Canary Current. The region of maximum freshening (by 35 psu) is in the Labrador Sea in the vicinity of the four

ocean cells at which freshwater is introduced (labeled B in Fig. 1). The coldest annual mean surface air temperatures (Fig. 10c) are centered over Baffin Bay (73°N, 65°W) and off the east coast of Greenland with as much as 6°C of cooling; in the boreal winter, temperatures over Baffin Bay show the largest anomaly with more than 20°C of cooling. North-central Greenland is cooled by
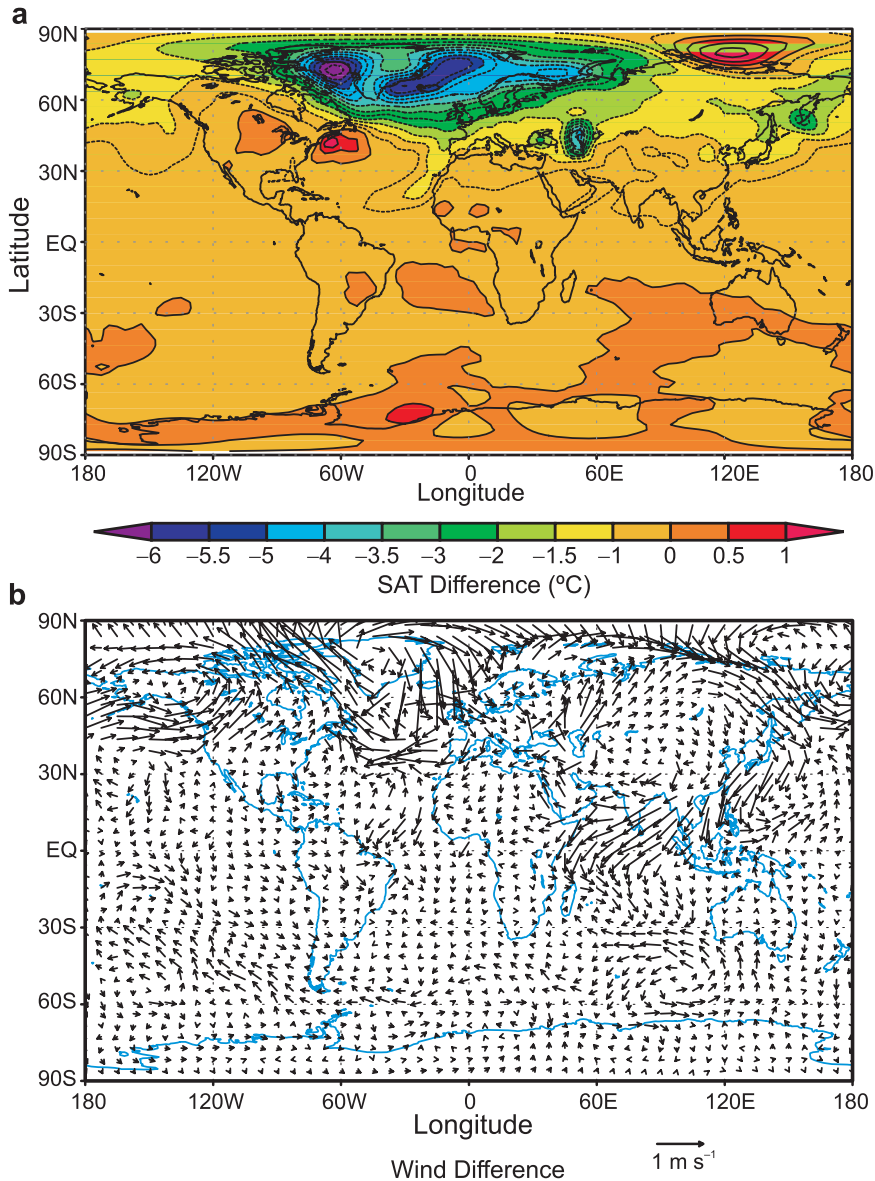
FIG. 11. Modeled global impacts of the flood event assuming forcing B + C. Results are averaged over postflood years 10–47. (a) Change in mean annual surface air temperature. (b) Change in mean annual surface wind field (m s^{-1}).

3°C and south-central Greenland by 3.5°C. Arctic Scandinavia is cooled by 3.5°–5°C and northwest Europe and the British Isles by 2°–3.5°C. A localized cooling of 4°C is centered on the Caspian Sea. Regions of ~1°C warming are located over the Laptev Sea (80°N, 120°E) and the Gulf of Maine (45°N, 60°W). Increased SSTs in the Laptev Sea result from a decrease in sea ice that is also related to changes in atmospheric circulation (more southerly flow brings warmer air temperatures there); increased SSTs in the Gulf of Maine are from a combination of changes in

wind stress curl and coastal upwelling. The mean annual temperature for most parts of North America is little affected. The spatial pattern of the modeled SAT anomaly is quite similar to that of the atmosphere–ocean coupled general circulation model (AOGCM) ensemble of CMIP shown in Stouffer et al. (2006, their Fig. 14) in which the impact of the winds and the wind-driven ocean circulation is clearly evident in the Canary Current and the gyre circulation of the North Atlantic but is not captured in the intermediate model ensemble.
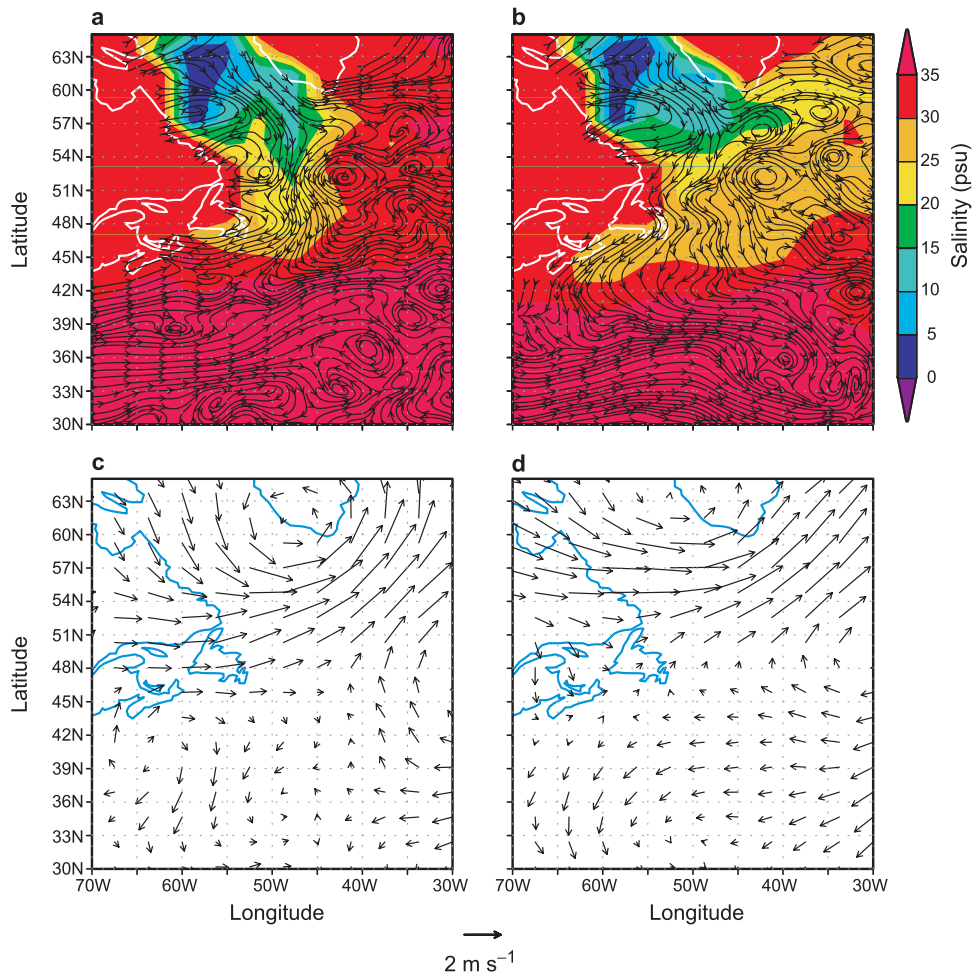
FIG. 12. Modeled impacts of the Agassiz flood in response to the B + C freshwater forcing. (a) Ocean salinity (psu) and streamlines of surface currents at model time $t = 1.58$ yr. (b) As for (a) but at model time $t = 4.92$ yr. (c) Wind vector difference (m s^{-1}) relative to control run at model time $t = 1.58$ yr. (d) As for (c) but at model time $t = 4.92$ yr.

Figure 10d shows that the modeled changes in sea ice thickness and extent are broadly consistent with the changes in SST and SSS. The greatest changes occur in Baffin Bay and in the Greenland Sea, with lesser changes in the Barents and Chuckchi Seas. Convection is suppressed in regions of expanded sea ice and enhanced at the sea ice margin. A conspicuous reduction of sea ice thickness, consistent with the modeled SAT, winds, SST, and SSS, is predicted for the Laptev Sea. Note that where much of the sea ice anomaly occurs there is strong correlation with the freshwater anomaly, so any impact on salinity would therefore be negligible.

The map of precipitation change (Fig. 10e) shows a complex pattern, but rough generalizations are possible. Most of Europe and Asia north of 40°N was drier during the cold event, whereas in North America there are areas of increased precipitation centered over

Oregon and Nova Scotia. For Greenland, the precipitation is decreased almost everywhere, including all the deep ice core sites. The largest snowfall anomalies (Fig. 10f) are located offshore where they would leave no proxy record. There is increased snowfall over the North American cordillera, the European Alps, and Scandinavia, so advances in mountain glaciers would be expected in these regions. The snowfall anomaly pattern over Greenland shows decreased snowfall over central Greenland and increased snowfall nearer the coast.

Changes in surface air temperature and wind vector are largely confined to the Northern Hemisphere (Fig. 11). As for Fig. 10 the plotted results have been averaged over postflood years 10–47. A slight warming in the South Atlantic (20°S, 20°W) might be construed as a very weak expression of hemispheric coupling associated with
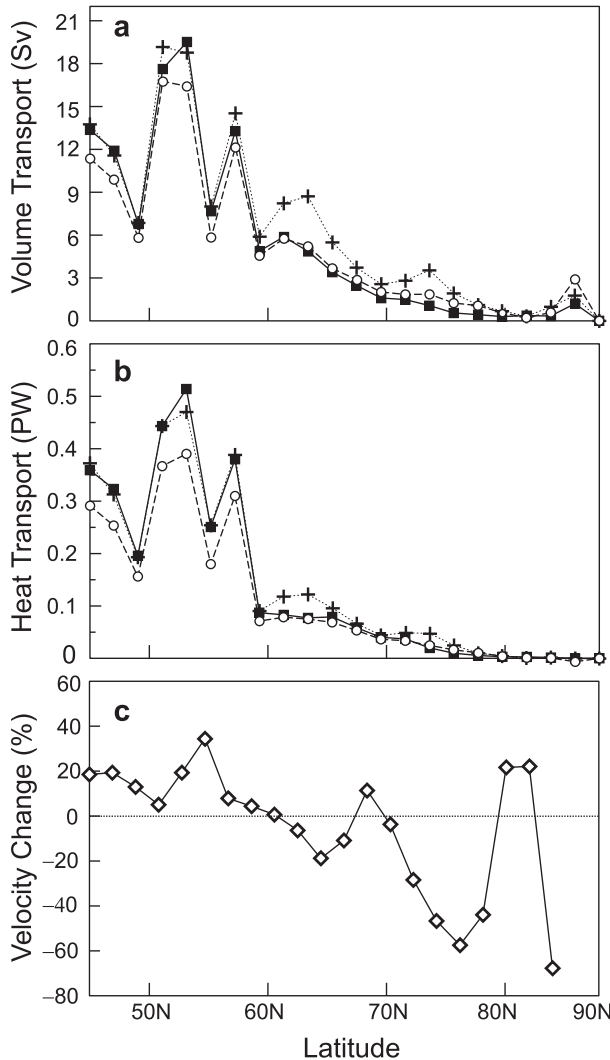
FIG. 13. Modeled changes in North Atlantic circulation. Results are averaged over 47 postflood years. (a) Northward volume transport (Sv). The modern control run is indicated by a dotted line with plus signs, the 8200 BP no-flood control run by a dashed line and open circles, and the response to the B + C forcing applied at 8200 BP by a solid line and solid squares. (b) Northward heat transport (PW). The modern control run is indicated by a dotted line with plus signs, the 8200 BP no-flood control run by a dashed line and open circles, and the response to the B + C forcing applied at 8200 BP by a solid line and solid squares. (c) Percentage change in southward velocity averaged over depths below 1279.1 m.

Atlantic Ocean circulation, which plays a major role in glacial climate variability (e.g., Knutti et al. 2004; EPICA Community Members et al. 2006); however, in contrast with the results of LeGrande and Schmidt (2008), we find the modeled change in northward heat transport in the equatorial Atlantic is small, varying from −4% to +8% within the 30°N–0° latitude band. The wind difference vector (Fig. 11b) over Greenland indicates enhanced

anticyclonic flow over the ice sheet and is consistent with colder temperatures and reduced precipitation. Over Southeast Asia, the characteristic westerly monsoon winds (that dominate the annual mean) are weakened.

Figure 12 is intended to clarify the mechanisms that transport freshwater from the Labrador Sea to high latitudes in the North Atlantic. The upper panels depict the sea surface salinity at times 1.58 and 4.92 yr after the flood onset. The lower panels illustrate mean annual changes in the wind vector at the same times. These plots were motivated by discussions with coastal ocean-ographers who expressed concern that the freshwater plume from Hudson Strait would remain trapped along the eastern seaboard of North America (e.g., Chapman 2000; Chapman and Lentz 1994) and therefore could not affect the SST and salinity of the North Atlantic. This trapping tendency is illustrated in Fig. 12b but when the plume encounters the North Atlantic drift it is swept northeastward toward the Nordic seas. Interest-ingly the model predicts an eastward freshwater flux around the southern tip of Greenland—opposite to the modern Irminger Current and a consequence of the modeled changes in the wind field.

Much of the modeling of abrupt climate events has been concerned with how the addition of freshwater to the upper ocean affects the poleward transport of heat in the North Atlantic. The main features of the modeled changes are illustrated in Fig. 13, and our focus is on the latitude de-pendence of northward volume transport $\mathcal{Q}$, the north-ward heat transport $\mathcal{H}$, and the change in cross-sectionally averaged southward flow velocity of the deep ocean $\overline{v_d}$. The modern control configuration is indicated by dotted lines and plus signs, the 8.2 ka BP control configuration by dashed lines and open circles, and the response to the B + C forcing by a solid line and solid squares (Figs. 13a,b). The percentage change in $\overline{v_d}$ relative to the control state is indicated by a solid line and open diamonds (Fig. 13c). The quantities are calculated as follows:

$$\mathcal{Q} = \int_A \max[v_N, 0] dA$$
$$\mathcal{H} = \int_A \rho_{sw} cT \max[v_N, 0] dA$$
$$\overline{v_d} = \frac{1}{A_d} \int_{A_d} \max[v_S, 0] dA_d,$$

where v_N and v_S are the north- and southward compo-nents of ocean velocity, A is the latitudinally varying cross-sectional area of the North Atlantic, A_d is the cross-sectional area below 1279.1m, ρ_{sw} is the temperature- and salinity-dependent density of ocean water, $c = 4.186$ kJ kg^{-1} K^{-1} is the specific heat capacity, and T is the Celsius temperature. The sign of $\overline{v_d}$ has been set so that

southward flow is positive and $\mathcal{Q}$, $\mathcal{H}$, and $\overline{v_d}$ have been averaged over 47 postflood years. (Analogous calculations to obtain the southward transport of $\mathcal{Q}$ and $\mathcal{H}$ yield results that are closely similar to those for northward transport.)

Comparison of the 8.2 ka BP control with the modern control indicates that the northward transport of volume was reduced by as much as 2 Sv (Fig. 13a) and the northward transport of heat by as much as 0.05 PW at 8.2 ka BP (Fig. 13b). Comparison of the 8.2 ka BP control with the ocean response to the B + C forcing reveals that the modeled differences between the 8.2 ka BP control and modern exceed those between the 8.2 ka BP control and the postflood response. Though these differences are small they are interesting. In the 45°–60°N latitude range the postflood transport of volume and heat is actually larger after the flood than before it because the wind-driven transport is increased after the flood. North of 60°N the volume transport seems to have decreased very slightly after the flood but the heat transport (which was already small) did not change significantly in magnitude; expressed as a percentage, there was an actual *increase* in northward heat transport by as much as 15%. To compare the simulation results with paleocurrent measurements of the Nordic seas overflow sites, we show the percentage changes in $\overline{v_d}$ as a function of latitude (Fig. 13c). The largest percentage reduction in deep southward flow (around 60%) occurs at 75°N and there is a negligible change in the range 57°–62°N.

c. Comparison with paleoenvironmental proxies

We concentrate attention on recent results from Greenland and the North Atlantic. Four deep ice cores from Greenland (Dye3, GRIP, GISP2, NGRIP) show a consistent $\delta^{18}O$ record of the 8.2 ka cooling, which is described as the "extreme event in the Holocene of all four cores" (Thomas et al. 2007), and of a decrease in snow accumulation rate. The best estimate of the associated cooling in central Greenland is $3.3 \pm 1.1°C$ (Kobashi et al. 2007), somewhat less than the ~5°C indicated by the spatially averaged B + C time series (Fig. 9a) but comparable to the time-averaged values in Fig. 10c. Thomas et al. (2007) comment that the changes in impurity ion concentrations in the ice cores are not large and take this as evidence that changes in atmospheric circulation were also not large. For the B + C model we find that anticyclonic flow around Greenland was substantially strengthened although the circulation over central Greenland was not greatly affected.

According to C. Hillaire-Marcel et al. (2008), the absence of a clear signal of Lake Agassiz drainage in deep-sea North Atlantic $\delta^{18}O$ records may be a consequence of the isotopic composition of the flood waters rather than evidence for the absence of temperature and salinity changes. Using foraminiferal $\delta^{18}O$ and Mg/Ca proxies, Came et al. (2007) find a ~2°C cooling and freshening in the vicinity of the Reykjanes Ridge south of Iceland. Our B + C model results (Fig. 10) show a freshening and a ~4.5°C SST decrease for the same region.

Farther afield, the model predicts a reduction in sea surface temperature and salinity off the coast of Portugal (see the southward-pointing finger of cold, freshwater in Figs. 10b,c) which is in agreement with the results of Duplessy et al. (1992) and hardly an obvious consequence of adding freshwater to the Labrador Sea. Interestingly, the model also predicts a weakening of the Indian monsoon, which is in agreement with a speleothem record from the Arabian Peninsula that shows a reduction in monsoon precipitation at the time of the 8.2 ka event (Fleitmann et al. 2003).

Sortable sediment proxies for Nordic seas overflow currents at sites on the Gardar Drift (57°26.87′N) (Ellison et al. 2006), Eirik Drift (57°26.56′N) (Kleiven et al. 2008), and Reykjanes Ridge (61°25′N) (Praetorius et al. 2008) suggest a reduced overflow around the time of the 8.2 ka event. Our simulations indicate a negligible change at these latitudes but a fractional reduction in flow of as much as 60% around 75°N.

5. Discussion and conclusions

Our preference for the B + C forcing model is based on the argument that the preflood outflow from Lake Agassiz, directed to the St. Lawrence estuary, had a high concentration of suspended sediment and that sedimentation from this fresh turbid layer drove a mixing process that actively removed freshwater from the upper ocean. As a result, discharge along this pathway would not contribute to surface freshening of the North Atlantic. As demonstrated by Parsons et al. (2001), this mixing process can become effective when the near-surface water density ρ (including sediment) is far less than the density of the underlying saline water ρ_{sw}. The issue is a significant one for paleoceanography and is currently being studied from experimental (A. M. Jellinek 2007, personal communication) and computational fluid dynamics (E. H. Meiburg 2007, personal communication) perspectives.

A further complicating, but potentially critical, factor that is also under investigation is the behavior of hyperpycnal flows in a stratified ambient. After the plume loses its sediment at depth it is unlikely to be able to return to the near surface if there is a pycnocline present above it

(H. Huppert 2007, personal communication); therefore no upper-ocean freshening would be possible in such a circumstance. This uncertainty clouds discussion of whether, during the flood phase, the outflow through Hudson Strait was also densely sediment laden. If this were the case, then the B forcing model could provide the best representation of the near-surface freshwater forcing of the Labrador Sea. We have simulated this situation as well but the results are not sufficiently different from the B + C model to merit additional figures and extended discussion. Comparison of the B + C and C time series in Fig. 9 indicates that the main contribution to the modeled climate response results from the postflood outflow through Hudson Strait (B forcing) and not from the flood pulse (C forcing). Thus the redirection of water from the Kinojévis–St. Lawrence routing to the Hudson Bay–Hudson Strait routing (with the additional assumption that the Kinojévis–St. Lawrence discharge was hyperpycnal) is essential for triggering the abrupt climate change event.

The B + C modeling results slightly overestimate the cooling of central Greenland and of North Atlantic SST. As previously noted, most of the modeled cooling is a consequence of the postflood outflow through Hudson Strait rather than the flood itself. Our value for postflood discharge is extracted from Licciardi et al. (1999) and is subject to considerable uncertainty. Reducing the postflood discharge through Hudson Strait would reduce the modeled climate impacts. After 47 postflood model years, Fig. 9 shows no evidence of recovery from the B + C freshwater forcing. Extending the duration of the model run is unlikely to change the situation. Thus the recovery must result from some additional change in the forcing, for example, a progressive reduction in the freshwater outflow through Hudson Strait or from external changes that we have not accounted for. The freshwater discharge into Hudson Bay (and hence the suspended sediment flux) declined as the Laurentide Ice Sheet wasted away, reaching modern values around 7000 ^{14}C yr BP (Licciardi et al. 1999).

Several modeling studies of the climate impacts of the Lake Agassiz flood have used ensemble modeling (Renssen et al. 2001; Bauer et al. 2004; LeGrande et al. 2006; LeGrande and Schmidt 2008) to examine the modeled sensitivity to initial conditions and the robustness of the conclusions reached. Because we have not followed this path, we cannot reach strong conclusions about the robustness of our results. Subject to this uncertainty, the main conclusions of this study are as follows: 1) Freshening of the North Atlantic can produce abrupt climate change events that are not associated with shutdown or substantial reduction of the poleward transport of ocean heat. 2) Transport of low-salinity near-surface water from a source region such as Hudson Strait to high latitudes in the North Atlantic Ocean can itself be sufficient to greatly increase the thickness and extent of sea ice and produce a rapid climate reversal. 3) To capture this process it is essential to use fully coupled atmosphere–ocean GCMs. Examples that support this claim include the following: the change in wind vector (e.g., Fig. 12) that results from the freshwater release can play an essential role in transporting freshwater to high-latitude regions of sea ice production; the spatial pattern of modeled SAT anomaly is quite similar to those produced by the AOGCM ensemble of CMIP shown in (Stouffer et al. 2006, Fig. 14) in which the impact of the winds and the wind-driven ocean circulation is clearly evident in the Canary Current and the gyre circulation of the North Atlantic but is not captured in the intermediate model ensemble. 4) Considering freshwater inputs without reference to their sediment load can lead to erroneous estimates of the ocean response to freshwater forcing. 5) The paleoturbidity of freshwater discharge to the oceans can be assessed using river modeling based on knowledge of paleohydrology and paleotopography and the marine sedimentary record.

REFERENCES

Aharon, P., 2006: Entrainment of meltwaters in hyperpycnal flows during deglaciation superfloods in the Gulf of Mexico. *Earth Planet. Sci. Lett.,* **241,** 260–270.

Alley, R. B., and A. M. Ágústsdóttir, 2005: The 8k event: Cause and consequences of a major Holocene abrupt climate change. *Quat. Sci. Rev.,* **24,** 1123–1149.

Barber, D. C., and Coauthors, 1999: Forcing of the cold event of 8,200 years ago by catastrophic drainage of Laurentide lakes. *Nature,* **400,** 344–348.

Bauer, E., A. Ganopolski, and M. Montoya, 2004: Simulation of the cold climate event 8200 years ago by meltwater outburst from Lake Agassiz. *Paleoceanography,* **19,** PA3014, doi:10.1029/2004PA001030.

Berger, A., and M. F. Loutre, 1991: Insolation values for the climate of the last 10 million years. *Quat. Sci. Rev.,* **10,** 297–317.

Bianchi, G. G., and I. N. McCave, 1999: Holocene periodicity in North Atlantic climate and deep ocean flow south of Iceland. *Nature,* **397,** 515–517.

Björnsson, H., 2003: Subglacial lakes and jökulhlaups in Iceland. *Global Planet. Change,* **35,** 255–271.

Bond, G., and Coauthors, 1992: Evidence for massive discharges of icebergs into the North Atlantic Ocean during the last glacial period. *Nature,* **360,** 245–249.

Boyle, E. A., and L. Keigwin, 1987: North Atlantic thermohaline circulation during the past 20,000 years linked to high-latitude surface temperature. *Nature,* **330,** 35–40.

Broecker, W. S., 1994: Massive iceberg discharges as triggers for global climate change. *Nature,* **372,** 421–424.

Bush, A. B. G., 2007: Extratropical influences on the El Niño–Southern Oscillation through the late Quaternary. *J. Climate,* **20,** 788–800.

Came, R. E., D. W. Oppo, and J. F. McManus, 2007: Amplitude and timing of temperature and salinity variability in the subpolar North Atlantic over the past 10 k.y. *Geology,* **35,** 315–318.

Chapman, D. C., 2000: A numerical study of the adjustment of a narrow stratified current over a sloping bottom. *J. Phys. Oceanogr.,* **30,** 2927–2940.

——, and S. J. Lentz, 1994: Trapping of a coastal density front by the bottom boundary layer. *J. Phys. Oceanogr.,* **24,** 1464–1479.

Clark, P. U., S. J. Marshall, G. K. C. Clarke, S. W. Hostetler, J. M. Licciardi, and J. T. Teller, 2001: Freshwater forcing of abrupt climate change during the last glaciation. *Science,* **293,** 283–287.

Clarke, G. K. C., 2003: Hydraulics of subglacial outburst floods: New insights from the Spring–Hutter formulation. *J. Glaciol.,* **49,** 299–313.

——, D. W. Leverington, J. T. Teller, and A. S. Dyke, 2004: Paleohydraulics of the last outburst flood from glacial Lake Agassiz and the 8200 BP cold event. *Quat. Sci. Rev.,* **23,** 389–407.

Duplessy, J. C., L. Labeyrie, M. Arnold, M. Paterne, J. Duprat, and T. C. E. van Weering, 1992: Changes in surface salinity of the North Atlantic Ocean during the last deglaciation. *Nature,* **358,** 485–488.

Dyke, A. S., A. Moore, and L. Robinson, 2003: Deglaciation of North America. Geological Survey of Canada Open File 1574, 2 pp.

Egbert, G. B., and R. D. Ray, 2000: Significant dissipation of tidal energy in the deep ocean inferred from satellite altimeter data. *Nature,* **405,** 775–778.

Ellison, C. R. W., M. R. Chapman, and I. R. Hall, 2006: Surface and deep ocean interactions during the cold climate event 8200 years ago. *Science,* **312,** 1929–1932.

EPICA Community Members, and Coauthors, 2006: One-to-one coupling of glacial climate variability in Greenland and Antarctica. *Nature,* **444,** 195–198.

Fanning, A. F., and A. J. Weaver, 1996: An atmospheric energy–moisture balance model: Climatology, interpendatal climate change, and coupling to an ocean general circulation model. *J. Geophys. Res.,* **101,** 15 111–15 128.

Fleitmann, D., S. J. Burns, M. Mudelsee, U. Neff, J. Kramers, A. Maginin, and A. Matter, 2003: Holocene forcing of the Indian monsoon recorded in a stalagmite from southern Oman. *Science,* **300,** 1737–1739.

Goosse, H., H. Renssen, F. M. Selten, R. J. Haarsma, and J. D. Opsteegh, 2002: Potential causes of abrupt climate events: A numerical study with a three-dimensional climate model. *Geophys. Res. Lett.,* **29,** 1860, doi:10.1029/2002GL014993.

Gordon, C. T., and W. F. Stern, 1982: A description of the GFDL global spectral model. *Mon. Wea. Rev.,* **110,** 625–644.

Hall, A., and R. J. Stouffer, 2001: An abrupt climate event in a coupled ocean–atmosphere simulation without external forcing. *Nature,* **409,** 171–174.

Hemming, S. R., 2004: Heinrich events: Massive late Pleistocene detritus layers of the North Atlantic and their global climate imprint. *Rev. Geophys.,* **42,** RG1005, doi:10.1029/2003RG000128.

Hillaire-Marcel, C., A. de Vernal, and D. J. W. Piper, 2007: Lake Agassiz final drainage event in the northwest North Atlantic. *Geophys. Res. Lett.,* **34,** L15601, doi:10.1029/2007GL030396.

——, J.-F. Hélie, J. McKay, and A. de Vernal, 2008: Elusive isotopic properties of deglacial meltwater spikes into the North Atlantic: Example of the final drainage of Lake Agassiz. *Can. J. Earth Sci.,* **45,** 1235–1242.

Hughen, K. A., J. T. Overpeck, L. C. Peterson, and S. Trumbore, 1996: Rapid climate changes in the tropical Atlantic region during the last deglaciation. *Nature,* **380,** 51–54.

——, ——, S. J. Lehman, M. Kashgarian, J. Southon, L. C. Peterson, R. Alley, and D. M. Sigman, 1998: Deglacial changes in ocean circulation from an extended radiocarbon calibration. *Nature,* **391,** 65–68.

Indermühle, A., and Coauthors, 1999: Holocene carbon-cycle dynamics based on CO_2 trapped in ice at Taylor Dome, Antarctica. *Nature,* **398,** 121–126.

Jayne, S. R., and L. C. St. Laurent, 2001: Parameterizing tidal dissipation over rough topography. *Geophys. Res. Lett.,* **28,** 811–814.

Keigwin, L. D., and E. A. Boyle, 2000: Detecting Holocene changes in thermohaline circulation. *Proc. Natl. Acad. Sci. USA,* **97,** 1343–1346.

——, J. P. Sachs, Y. Rosenthal, and E. A. Boyle, 2005: The 8200 year B.P. event in the slope water system, western subpolar North Atlantic. *Paleoceanography,* **20,** PA2003, doi:10.1029/2004PA001074.

Kerwin, M. W., 1996: A regional stratigraphic isochron (ca. 8000 ^{14}C yr B.P.) from final deglaciation of Hudson Strait. *Quat. Res.,* **46,** 89–98.

Kleiven, H. F., C. Kissel, C. Laj, U. S. Ninnemann, T. O. Richter, and E. Cortijo, 2008: Reduced North Atlantic deep water coeval with glacial Lake Agassiz freshwater outburst. *Science,* **319,** 60–64.

Klitgaard-Kristensen, D., H. P. Sejrup, H. Haflidason, S. Johnsen, and M. Spurk, 1998: A regional 8200 cal. yr BP cooling event in northwest Europe, induced by final stages of the Laurentide ice-sheet deglaciation? *J. Quat. Sci.,* **13,** 165–169.

Knutti, R., J. Flückiger, T. F. Stocker, and A. Timmermann, 2004: Strong hemispheric coupling of glacial climate through freshwater discharge and ocean circulation. *Nature,* **430,** 851–856.

Kobashi, T., J. P. Severinghaus, E. J. Brook, J.-M. Barnola, and A. M. Grachev, 2007: Precise timing and characterization of abrupt climate change 8200 years ago from air trapped in polar ice. *Quat. Sci. Rev.,* **26,** 1212–1222.

Ledwell, J. R., A. J. Watson, and C. S. Law, 1998: Mixing of a tracer released in the pycnocline. *J. Geophys. Res.,* **103,** 21 499–21 529.

LeGrande, A. N., and G. A. Schmidt, 2008: Ensemble, water isotope–enabled, coupled general circulation modeling insights into the 8.2 ka event. *Paleoceanography,* **23,** PA3207, doi:10.1029/2008PA001610.

——, ——, D. T. Shindell, C. V. Field, R. L. Miller, D. M. Koch, G. Faluvegi, and G. Hoffmann, 2006: Consistent simulations of multiple proxy responses to an abrupt climate change event. *Proc. Natl. Acad. Sci. USA,* **103,** 837–842.

Lehman, S. J., and L. D. Keigwin, 1992: Sudden changes in North Atlantic circulation during the last deglaciation. *Nature,* **356,** 757–762.

Leverington, D. W., and J. T. Teller, 2003: Paleotopographic reconstructions of the eastern outlets of glacial Lake Agassiz. *Can. J. Earth Sci.,* **40,** 1259–1278.

Levitus, S., 1982: *Climatological Atlas of the World Ocean.* NOAA Professional Paper 13, 173 pp.

Licciardi, J. M., J. T. Teller, and P. U. Clark, 1999: Freshwater routing by the Laurentide ice sheet during the last deglaciation. *Mechanisms of Global Climate Change at Millennial Time Scales,* P. U. Clark et al., Eds., Amer. Geophys. Union, 177–202.

Martin, D., and R. Nokes, 1988: Crystal settling in a vigorously convecting magma chamber. *Nature,* **332,** 534–536.

McManus, J. F., R. Francois, J.-M. Gherardi, L. D. Keigwin, and S. Brown-Leger, 2004: Collapse and rapid resumption of Atlantic meridional circulation linked to deglacial climate change. *Nature,* **428,** 834–837.

Meehl, G. A., P. R. Gent, J. M. Arblaster, B. L. Otto-Bleisner, E. C. Brady, and A. Craig, 2001: Factors that affect the amplitude of El Niño in global coupled climate models. *Climate Dyn.,* **17,** 515–526.

Menounos, B., J. Koch, G. Osborn, J. J. Clague, and D. Mazzucchi, 2004: Early Holocene glacier advance, southern Coast Mountains, British Columbia, Canada. *Quat. Sci. Rev.,* **23,** 1543–1550.

Navarra, A., W. F. Stern, and K. Miyakoda, 1994: Reduction of the Gibbs oscillation in spectral model simulations. *J. Climate,* **7,** 1169–1183.

Nesje, A., and D. O. Dahl, 2001: The Greenland 8200 cal. yr BP event detected in loss-on-ignition profiles in Norwegian lacustrine sediment sequences. *J. Quat. Sci.,* **16,** 155–166.

Pacanowski, R. C., 1995: MOM2 documentation, user's guide, and reference manual. GFDL Ocean Group Tech. Rep. 3, 232 pp.

——, and S. G. H. Philander, 1981: Parameterization of vertical mixing in numerical models of tropical oceans. *J. Phys. Oceanogr.,* **11,** 1443–1451.

Parsons, J. D., J. W. M. Bush, and J. P. M. Syvitski, 2001: Hyperpycnal plume formation from riverine outflows with small sediment concentrations. *Sedimentology,* **48,** 465–478.

Peltier, W. R., 1994: Ice age paleotopography. *Science,* **265,** 195–201.

——, 1998: Postglacial variations in the level of the sea: Implications for climate dynamics and solid-earth geophysics. *Rev. Geophys.,* **36,** 603–689.

Praetorius, S. K., J. F. McManus, D. W. Oppo, and W. B. Curry, 2008: Episodic reductions in bottom water currents since the last ice age. *Nature Geosci.,* **1,** 449–452.

Rensssen, H., H. Goose, T. Fichefet, and J.-M. Campin, 2001: The 8.2 kyr BP event simulated by a global atmosphere–sea-ice–ocean model. *Geophys. Res. Lett.,* **28,** 1567–1570.

——, ——, and ——, 2002: Modeling the effect of freshwater pulses on the early Holocene climate: The influence of high-frequency climate variability. *Paleoceanography,* **17,** 1020, doi:10.1029/2001PA000649.

——, ——, and ——, 2007: Simulation of Holocene cooling events in a coupled climate model. *Quat. Sci. Rev.,* **26,** 2019–2029.

Roche, D. M., H. Renssen, S. L. Weber, and H. Goosse, 2007: Could meltwater pulses have been sneaked unnoticed into the deep ocean during the last glacial? *Geophys. Res. Lett.,* **34,** L24708, doi:10.1029/2007GL032064.

Rohling, E. J., and H. Pälike, 2005: Centennial-scale climate cooling with a sudden cold event around 8,200 years ago. *Nature,* **434,** 975–979.

Saucier, F. J., S. Senneville, S. Prinsenberg, F. Roy, G. Smith, P. Gachon, D. Caya, and R. Laprise, 2004: Modelling the sea ice-ocean seasonal cycle in Hudson Bay, Foxe Basin and Hudson Strait, Canada. *Climate Dyn.,* **23,** 303–326.

Schiesser, W. E., 1991: *The Numerical Method of Lines: Integration of Partial Differential Equations.* Academic Press, 326 pp.

Seager, R., and D. S. Battisti, 2007: Challenges to our understanding of the general circulation: Abrupt climate change. *Global Circulation of the Atmosphere,* T. Schneider and A. H. Sobel, Eds., Princeton University Press, 331–371.

——, ——, J. Yin, N. Gordon, N. Naik, A. C. Clement, and M. A. Cane, 2002: Is the Gulf Stream responsible for Europe's mild winters? *Quart. J. Roy. Meteor. Soc.,* **128,** 2563–2586.

Seppä, H., and Coauthors, 2007: Spatial structure of the 8200 cal yr BP event in Northern Europe. *Climate Past,* **3,** 165–195.

Simmons, H. L., S. R. Jayne, L. C. S. Laurent, and A. J. Weaver, 2004: Tidally driven mixing in a numerical model of the ocean general circulation. *Ocean Modell.,* **6,** 245–263.

Spooner, I., M. S. V. Douglas, and L. Terrusi, 2002: Multiproxy evidence of an early Holocene (8.2 kyr) climate oscillation in central Nova Scotia, Canada. *J. Quat. Sci.,* **17,** 639–645.

St-Onge, G., and P. Lajeunesse, 2007: Flood-induced turbidites from northern Hudson Bay and western Hudson Strait: A two-pulse record of Lake Agassiz final outburst flood? *Submarine Mass Movements and Their Consequences,* V. Lykousis et al., Eds., Advances in Natural and Technological Hazards Research Series, Vol. 27, Springer, 129–137.

——, J. S. Stoner, and C. Hillaire-Marcel, 2003: Holocene paleomagnetic records from the St. Lawrence Estuary, eastern Canada: Centennial- to millennial-scale geomagnetic modulation of cosmogenic isotopes. *Earth Planet. Sci. Lett.,* **209,** 113–130.

Stouffer, R. J., and Coauthors, 2006: Investigating the causes of the response of the thermohaline circulation to past and future climate changes. *J. Climate,* **19,** 1365–1387.

Straneo, F., and F. Saucier, 2008: The outflow from Hudson Strait and its contribution to the Labrador Current. *Deep-Sea Res.,* **55,** 926–946.

Tarasov, L., and W. R. Peltier, 2005: Arctic freshwater forcing of the Younger Dryas cold reversal. *Nature,* **435,** 662–665.

Teller, J. T., and D. W. Leverington, 2004: Glacial Lake Agassiz: A 5000 yr history of change and its relationship to the $\delta^{18}O$ record of Greenland. *Geol. Soc. Amer. Bull.,* **116,** 729–742.

——, ——, and J. D. Mann, 2002: Freshwater outbursts to the oceans from glacial Lake Agassiz and climate change during the last deglaciation. *Quat. Sci. Rev.,* **21,** 879–887.

Thomas, E. R., and Coauthors, 2007: The 8.2 ka event from Greenland ice cores. *Quat. Sci. Rev.,* **26,** 70–81.

Thompson, L., and Coauthors, 2002: Kilimanjaro ice core records: Evidence of Holocene climate change in tropical Africa. *Science,* **298,** 589–593.

Trenberth, K. E., and J. M. Caron, 2001: Estimates of meridional atmosphere and ocean heat transports. *J. Climate,* **14,** 3433–3443.

van Geel, B., J. van der Plicht, and H. Renssen, 2003: Major Δ^{14}C excursions during the late glacial and early Holocene: Changes in ocean ventilation or solar forcing of climate change? *Quat. Int.,* **105,** 71–76.

Veski, S., H. Seppä, and A. E. K. Ojala, 2004: Cold event at 8200 yr B.P. recorded in annually laminated lake sediments in eastern Europe. *Geol. Soc. Amer. Bull.,* **32,** 681–684.

von Grafenstein, U., H. Erlenkeuser, J. Müller, J. Jouzel, and S. Johnsen, 1998: The cold event 8200 years ago documented in oxygen isotope records of precipitation in Europe and Greenland. *Climate Dyn.,* **14,** 73–81.

Wetherald, R. W., and S. Manabe, 1988: Cloud feedback processes in a general circulation model. *J. Atmos. Sci.,* **45,** 1397–1415.

Wiersma, A. P., and H. Renssen, 2006: Model–data comparison for the 8.2 ka BP event: Confirmation of a forcing mechanism by catastrophic drainage of Laurentide lakes. *Quat. Sci. Rev.,* **25,** 63–88.

——, ——, H. Goosse, and T. Fichefet, 2006: Evaluation of different freshwater forcing scenarios for the 8.2 ka BP event in a coupled climate model. *Climate Dyn.,* **27,** 831–849.